The DOI for this manuscript is doi: 10.1175/JTECH-D-13-00083.1

Fietzek, P., B. Fiedler, T. Steinhoff, and A. Körtzinger, 2013: In situ quality assessment of a novel underwater pCO2 sensor based on membrane equilibration and NDIR spectrometry. J. Atmos. Oceanic Technol. doi:10.1175/JTECH-D-13-00083.1, in press.

In situ quality assessment of a novel underwater pCO_2 sensor based on membrane equilibration and NDIR spectrometry

Peer Fietzek[1]
GEOMAR Helmholtz Centre for Ocean Research Kiel, Kiel, Germany
and CONTROS Systems & Solutions GmbH, Kiel, Germany

Björn Fiedler, Tobias Steinhoff and Arne Körtzinger
GEOMAR Helmholtz Centre for Ocean Research Kiel, Kiel, Germany

[1] *Corresponding author address*: Peer Fietzek, GEOMAR Helmholtz Centre for Ocean Research Kiel, Düsternbrooker Weg 20, 24105 Kiel, Germany.
E-mail: pfietzek@geomar.de

Abstract

We present a detailed quality assessment of a novel underwater sensor for the measurement of CO_2 partial pressure (pCO_2) based on surface water field deployments carried out between 2008 and 2011. The commercially available sensor, which is based on membrane equilibration and NDIR spectrometry is small and can be integrated into mobile platforms. It is calibrated in water against a proven flow-through pCO_2 instrument within a custom-built calibration setup. The aspect of highest concern with respect to achievable data quality of the sensor is the compensation for signal drift inevitably connected to absorption measurements. We use three means to correct for drift effects: (i) a filter correlation or dual-beam setup, (ii) regular zero gas measurements realized automatically within the sensor and (iii) a zero-based transformation of two sensor calibrations flanking the time of sensor deployment.

Three sensors were tested against an underway pCO_2 system during two major research cruises providing an in situ temperature range from 7.4 to 30.1°C and pCO_2 values between 289 and 445 µatm. The average difference between sensor and reference pCO_2 was found to be -0.6 ± 3 µatm with a RMSE of 3.7 µatm.

1. Introduction

The measurement of dissolved carbon dioxide (CO_2) in seawater is important and valuable for a large number of scientific, industrial as well as socio-economic issues. Major scientific interest is related to the anthropogenic increase of atmospheric CO_2 concentrations and the resulting oceanic uptake of this most important anthropogenic greenhouse gas (Sabine et al. 2004; Rogner et al. 2007). The exchange of CO_2 across the air-sea interface and the dynamics and trends of the carbon cycle in coastal and open ocean regions (Takahashi et al. 2009; Gruber et al. 2010) as well as in the interior ocean are key aspects of current marine carbon cycle research.

Dissolved CO_2 reacts with water to form carbonic acid (H_2CO_3), which rapidly dissociates into hydrogen (H^+), bicarbonate (HCO_3^-), and carbonate ions (CO_3^{2-}). The exact speciation within the marine CO_2 system, i.e. between the above species of the carbonic acid dissociation system, strongly affects the pH of seawater (Millero 2007) and is of major interest. An increasing amount of dissolved CO_2 therefore leads to a decreasing pH, a process also referred to as ocean acidification in the context of the anthropogenic CO_2 transient. Its impact on calcifying organisms as well as on the physiology and reproduction of other marine species is presently not well understood (Doney et al. 2009). The potential long-term influence of acidification on fisheries but also carbon capture and underwater storage scenarios (IPCC 2005) show the socio-economic relevance of CO_2 measurements and highlight the demand for baseline monitoring of CO_2 parameters in the ocean.

Since the thermodynamic constants of the marine carbonate systems are known rather precisely (e.g., Millero 2007), the marine CO_2 system can be fully determined by

measurement of any two of the following variables: dissolved inorganic carbon (DIC), total alkalinity (TA), pH and CO_2 fugacity (fCO_2) or CO_2 partial pressure (pCO_2; Millero 2007). Although the sole measurement of pCO_2 is not sufficient to fully characterize the marine CO_2 system, pCO_2 is still a useful parameter on its own: It is the determining factor for air-sea gas exchange and responds sensitively to biogeochemical processes such as photosynthesis and respiration. Hence pCO_2 is both, a valuable stand-alone measurement parameter and a useful measured variable within multi-parameter measurements for the determination of the CO_2 system. So far only pCO_2 and pH can be measured autonomously with commercial underwater sensors (DeGrandpre et al. 1995; Seidel et al. 2008; Martz et al. 2010). Sensors for autonomous measurements of the other carbonate system parameters TA and DIC (Byrne et al. 2002; Wang et al. 2007) and even for direct measurements of carbonate ions are under development (Byrne and Yao 2008).

Due to a lack of a commercially available underwater pCO_2 sensor with a sufficient accuracy and platform integratability expressed by adequate dimensions, an appropriately short response time at surface and at depth as well as by the ability for continuous measurements, we have advanced the development of an autonomous and commercially produced underwater pCO_2 sensor (HydroC-CO_2, CONTROS GmbH, Kiel, Germany). Its versatility and specifications allow for integration into various platforms and provide a suitable tool for pCO_2 measurements at an improved spatial and temporal resolution in the water column. Here, we present a comprehensive overview of the sensor's measurement principle, its key components and its calibration. We also assess the achievable data quality by means of a detailed analysis of data from surface water field applications. Measurements against a proven flow-through system only represent

one application of the sensor, but at the same time enable the clearest assessment of the sensors data quality. Many further applications in the water column are possible and best require a dedicated discussions such as the measurements on a profiling float presented in Fiedler et al. (2013).

a. Suitable sensor platforms

Beside classical mobile sensor platforms on the one hand, such as voluntary observing ships (VOS) or research vessels, and stationary buoys and moorings on the other hand, innovative mobile platforms are receiving growing interest (Fietzek et al. 2011). These platforms, e.g. autonomous underwater vehicles (AUV), profiling floats and gliders, provide an increased autonomy, mobility and versatility as opposed to the classical carriers. They allow for a more cost-efficient data collection on so far largely unexplored temporal and spatial scales. These newly accessible scales are of high interest for the investigation of various biogeochemical processes, making these modern mobile platforms desirable carriers for pCO_2 sensors (Gruber et al. 2010). By equipping autonomous platforms as a regional or global sensor array with high spatiotemporal resolution, such as the prominent Argo project, a high scientific potential can be achieved (Roemmich et al. 2009; Johnson et al. 2009; Fiedler et al. 2013). However, in order to be easily installed on modern mobile platforms, new sensors need to cope with the demands of the more complex carriers and fulfill the more stringent requirements with respect to payload capacity, power availability, response time, etc. A more detailed discussion of these facts and circumstances can be found in Fietzek et al. (2011).

b. pCO_2 measurements

The first measurements of dissolved CO_2 were developed for medical applications in the 1950's. These were based on wet-chemical pH-determination behind a Teflon™ membrane (Stow et al. 1957; Severinghaus and Bradley 1958). Today optical CO_2 measuring techniques are prevailing. One method is to detect and quantify CO_2 molecules within an equilibrated gas stream by means of direct absorption in the infra red (IR) region of the electromagnetic spectrum. Another technique is an indirect measurement making use of the pH affecting property of CO_2 by applying spectrophotometry within an equilibrated pH-sensitive dye solution of known characteristics (DeGrandpre et al. 1995; Lefèvre et al. 1993). An overview of current sensor techniques for carbonate system species can be found in Byrne et al. (2010). A technical evaluation of pCO_2 sensors that also includes two sensors of the type discussed here is presented in Tamburri et al. (2011). Between the evaluation and the measurements discussed herein the status of the sensors was mainly improved through an optimized calibration process and data processing.

The usage of underway flow-through instruments to measure pCO_2 both in the oceanic surface layer and in the atmosphere dates back to the 1960s (Takahashi 1961). While in the beginning the application of these systems was restricted to research vessels, current, improved systems are suitable also for application on unattended platforms such as VOS (Watson et al. 2009; Pierrot et al. 2009; Pfeil et al. 2013). Continuous optimization of the overall setup and the components used lead to some standardized design that is nowadays also commercially available. The key components of such a flow-through instrument are the air-seawater equilibrator and the IR gas analyzer. The

equilibrator is used to achieve partial pressure equilibrium between the dissolved gases in a continuous stream of sea water and air that is re-circulated between the equilibrator and a benchtop IR analyzer. The achievable measuring accuracy is 2 µatm for surface seawater pCO_2 measurements (Pierrot et al. 2009). The flow-through system data are commonly reported as pCO_2 although the fCO_2 is the value suggested for most accurate carbonate system calculations. Based on approximated expressions the fCO_2, which considers the slightly non-ideal behavior of CO_2 in the gas phase, can be calculated from temperature and pCO_2, which presumes ideal gas behavior.

2. Sensor principle and description

a. Development and design

The development aims of the pCO_2 sensor among others were to obtain (i) a versatile and autonomous sensor that could be deployed on a profiling float with (ii) a response time of less than 5 min, (iii) an accuracy better 5 µatm, and (iv) a stability and reliability that would allow for long-term deployments of several months.

Since the developed sensor is based on the same measuring principle as proven flow-through systems, it has the same key components: an equilibrator and an IR CO_2 detector. A planar, semi-permeable membrane with a silicone active layer is installed in the head of the sensor. It acts as an equilibrator as well as a phase separator between the ambient water and an internal headspace. The sensor is commonly equipped with a water pump that provides a continuous seawater flow to the membrane and thus reduces the thickness of the static boundary layer in front of the membrane. By that, the response time is effectively shortened and made independent of a relative movement between the

membrane and the surrounding water. In order to withstand high hydrostatic pressures the membrane is mechanically supported from behind with a sintered metal disc. A gas pump continuously circulates air between the membrane equilibrator and a non-dispersive IR detector (NDIR). Figure 1 shows a model of the sensor and provides a schematic overview of its setup. The gas tightness of the internal gas stream as well as of the integrated valves is checked thoroughly prior to calibration. Opposed to pCO_2 underway systems in which gas stream leakages are a major source for measuring errors (Pierrot et al. 2009), the biggest "leak" within the gas stream of this sensor remains the equilibration membrane; the high gas permeability of the membrane related to the volume of the gas stream compensates for possible influences caused by small leaks. If bigger leakage occurs within the gas stream, the entire, much larger internal gas volume of the sensor will be equilibrated, leading to noticeably slower response times but not necessarily biases. The gas circuit also features a specially developed gas heater upstream of the NDIR detector whose heating control system is also used to stabilize the temperature of the IR detector. The gas heater buffers seawater temperature gradients ($\Delta T_{\text{in-situ}}$) in such a way that large $\Delta T_{\text{in-situ}}$ are damped to a much smaller gas temperature gradient. We choose to set the control temperature just high enough for the heating control circuit to keep the controlled temperature stable even at the maximum in situ temperature expected during deployment. When the control temperature is set higher than necessary, avoidably high power consumption is the consequence and the abundant absolute temperature differences between the surrounding water and the internal gas becomes larger. In addition to the gas heater and the temperature stabilization, the sensor's pressure housing is thermally insulated and temperature sensitive components are separately protected.

Within the gas stream sensors for pressure, temperature and relative humidity (RH) are installed to determine the conditions within the NDIR detector as well as behind the membrane. Their exact position was chosen upon laboratory tests to be most beneficial for their consideration within the IR sensor data analysis. The quality and a deep understanding of the NDIR detector are crucial for the data quality of both, underway instruments as well as the new underwater sensor. All additional components within the underway instrument's and the underwater sensor's gas circuit beside the equilibrator and NDIR detector, such as the additional sensors mentioned above, are required for accurate and precise absorption measurements and allow for preferably long deployments.

In contrast to common practice of underway instruments the absorption measurement within the sensor is carried out in wet air and without interrupting the gas flow for measurement. In the underwater sensor regular zero gas measurements can be carried out. Therefore valves are included into the circuit that lead the pumped air through a soda lime cartridge instead of the membrane equilibrator at desired intervals (see Fig. 1). In the presence of water vapor soda lime scrubs the CO_2 binding it as calcium carbonate ($CaCO_3$) thus creating a zero gas with respect to CO_2.

The sensor operates by consecutively switching through different intervals, the durations of which can be individually set. As soon as the sensor is powered it starts with a warm-up interval followed by continuous repetition of measuring cycles. One measuring cycle consists of three intervals: zero, flush and measure. The warm-up interval is only passed through once after the sensor has been turned on. The required warm-up time depends on the water temperature and the supplied voltage (c.f. Table 1).

191 During the warm-up, the water pump is disabled and data are neither transmitted nor
192 stored in the internal logger. During zero intervals, a zero CO_2 gas is created as described
193 above and the sensor provides the current zero reading used later for drift correction. The
194 zeroing typically lasts a few minutes and repetition is recommended at least every 12 h.
195 Data stored during that time are flagged for easy handling during analysis. Flush intervals
196 are only used to flag data acquired during the signal recovery from the zero value to the
197 ambient pCO_2 reading. Technically the measuring process of the sensor does not differ
198 between the flush and the subsequent measuring interval. The time the sensor needs for
199 full equilibration depends on the sensor configuration and the environmental conditions,
200 mainly the water temperature. The warmer the water, that faster the response time and
201 thus the shorter the required flush time. Laboratory and field tests for the response time
202 determination of the sensor as configured within the deployments presented here indicate
203 a linear dependency of response time on water temperature at a slope of the order of -1 s
204 per 1 °C (data not shown here). Sensor response to a step input can be well described by
205 first order kinetics and a corresponding exponential fit. Any response time given here
206 hence represents a time constant or a $t_{63\%}$ depending on which formulation is favored.
207 Isothermal pressure vessel experiments up to 200 bar have neither shown indications for a
208 pressure hysteresis, nor could a significant pressure influence on the response time be
209 identified (data not shown here).The actual response time of the sensor can be derived
210 based on the course of the signal recovery during the flush interval as applied by Fiedler
211 et al. (2013). It is typically faster than the 2 min response time of the flow-through system
212 (Pierrot et al. 2009) and allows for measurements on moving platforms; especially when
213 a response time correction is applied to derive the “true” ambient pCO_2 from the time-

lagged sensor signal (Fiedler et al. 2013). A more detailed analysis of the sensor's response characteristics is in preparation. During flush and measurement intervals, the water pump is active and data are recorded as configured. The interval settings simplify the data processing and provide the means to generate measurement data from a fully equilibrated and internally temperature stabilized sensor. Figure 2 shows the sensor signal during calibration with the zero, flush and measurement intervals indicated.

The comparatively fast response time, small size and operability of the sensor allow for deployments on various platforms. Due to its design and compared to classical flow-through systems the maintenance intensity and the risk for leaks in the gas stream are low. If used in situ, the sensor lacks the demand for an accurate water temperature probe as it is crucial for typical flow-through systems (Körtzinger et al. 2000). In order to derive the actual amount of dissolved CO_2 from the measured partial pressure, the sensor is commonly deployed together with a CTD probe, as the solubility of CO_2 depends on temperature and salinity (Weiss 1974).

b. Specifications

Table 1 lists the specifications of the developed sensor as applicable for the measurements discussed in this work. Different data communication options are feasible. An internal data logger is optional that can either be used as a stand-alone memory (e.g. Saderne et al. 2013) or for backup storage (e.g. Fiedler et al. 2013). A sleep mode function further facilitates autonomous installations. The sensor development also comprised a surface water flow-through version of the sensor which is not further addressed here.

c. CO_2 measurements by means of NDIR spectrometry

The properties of the NDIR detector are relevant for the overall performance of the sensor. Drift, cross-sensitivities and the signal-to-noise ratio (S/N) of the NDIR detector directly affect the data quality.

NDIR spectrometry in general is a proven direct measuring technique for mole fractions of gases absorbing in the IR. It is non-destructive and traceable to standards. NDIR detectors for CO_2 have small dimensions (several cm) and moderate power consumption (here: about 0.5 W) that allow for easy integration. In addition they provide good mechanical strength and are unaffected by vibrations if realized without moving parts. Due to their high selectivity and limited cross sensitivity NDIR detectors are well suited for qualitative analysis. NDIR detectors are composed of three main components: light source, absorption/beam path and detector. Each of them has different influences on the final sensor signal and depends differently on environmental variables, e.g. temperature. This may lead to complex overall sensor properties. Their choice defines the S/N, the sensitivity and the measurement range (detection limit and upper range value) of an NDIR unit. The basic idea is to get enough light energy at the desired wavelength to the detector and to make the absorption path sufficiently long such that changes in absorbed light intensity can be clearly resolved by the detector and amplifying electronics. Various options exist to optimize and dovetail these components.

The linear relation between the transmitted light intensity, I, and molecule concentration, c, as described by the Beer–Lambert Law makes the technique suitable for quantitative analysis:

$$I = I_0 10^{-\varepsilon c l} \quad , \tag{1}$$

with I_0 being the initial light intensity, l the distance the light travels through the absorbing medium and ε the molar absorption or extinction coefficient of the target molecule to be detected. According to (1) the extinction or absorbance, A, is defined to be directly proportional to the molecule concentration in the medium:

$$A = \log\left(\frac{I_0}{I}\right) = \varepsilon c l \,. \tag{2}$$

In reality there is a small non-linearity between the absorbance measured by the NDIR detector and molecule concentration due to the fact that the Beer–Lambert law is only defined for a single wavelength of infinitesimal small width, while in applications spectral dependencies occur (Wiegleb et al. 2001).

The NDIR unit used features a black body radiator as a broad band IR light source and a pyro-electrical IR detector which requires pulsed operation of the IR emitter. Interference filters in front of the detectors select the desired measurement as well as reference wavelength and together with electronics for control and evaluation complete the single beam dual wavelength NDIR detector. CO_2 is typically sensed around 4.26 µm where it shows its highest absorption due to its fundamental asymmetric stretching vibration (2349.1 cm^{-1}) and the reference wavelength is chosen to be placed in the water vapor window at around 4.0 µm.

Within an NDIR detector, several temperature influences exist that either require a compensation, calibration or stabilization. The spectral properties of the filters are temperature dependent: The central filter wavelength can shift as well as the transmission width can vary. A temperature influence on the sensor can occur in the form of thermal noise, a thermal background signal and changes in sensitivity. In the case of a dual beam setup the influences might even be different for both channels. The emission properties

and emitted intensities of the light source show a temperature influence as well. Thermal expansion of the cuvette or other mechanical deformations of the absorption path may have an additional effect on the measurements. Finally temperature dependencies of the analog electrical components directly behind the detector need to be considered. The overall effect caused by temperature changes is hence both variable in magnitude and sign for measurement channels of two similar products as well as for a measurement and reference channel within the same instrument with separate filters, detectors and electronics. For this reason and in order to enhance the measurement quality, the entire NDIR detector is temperature stabilized within the sensor. An active temperature stabilization furthermore helps to reduce the required warm-up time present in any NDIR detector due to self heating effects. A separation of the light source and the detector from the gas stream by windows enhances the temperature stabilization capability and protects the sensitive detector with the filter. A gas heater further reduces the temperature gradient within the cuvette and simultaneously reduces the risk of condensation within the optical components of the sensor.

Any sensor based on an absorption principle such as an NDIR detector senses the highest raw signal in the case of a complete absence of the target molecules in the beam path as in that case no absorption occurs and the maximum radiation intensity reaches the detector (see (1)). Therefore the regular determination of the sensor signal of a zero gas, the *zeroing*, is essential to account for drift effects that alter the light intensity with time and that otherwise would be erroneously interpreted as changes in target gas concentration. Typical effects are:

(i) Intensity variations or spectral shifts of the light source over time,

(ii) Contamination of any component within the beam path that might cause shadowing or growing reflectivity losses in the cuvette,

(iii) Aging effects that alter the detector sensitivity over time,

(iv) Changes in the pre-amplifier gain of the detector.

Within the sensor the zeroing does not only account for long-term drift influences but also for changes of the measurement conditions such as large changes in water temperature that cause internal temperature gradients and different water vapor concentrations within the gas stream.

Drift compensation by means of a differential setup in our case realized in the form of filter correlation is referred to as a two-beam/two-wavelength method. It is supposed to compensate any unwanted influences that cause signal drift of both channels in the same manner (aspects (i) and (ii) above) as the measured signal is continuously referenced. Any effects that cause changes in the detector signals and that are not caused by actual concentration changes within the cuvette shall be compensated in real time and parallel to measurements. In reality, this technique has its limitations in accounting for influences resulting from the usage of the two different channels with their own filters and detectors. Theoretically the zero-point of a two-beam instrument should not be affected by the above mentioned drift reasons ((i) through (iv)). But as we measure at two different wavelengths, spectral differences as well as effects related to the two physically different detectors still affect the zero signal of the “two-beam corrected” signal. Therefore we combine the zeroing and the two-beam drift correction means within our sensor. The latter provides a continuous correction applied parallel to measurements, while the zeroing discontinuously further enhances the drift correction capabilities by

328 correcting for effects that differently affect the measured intensities at both detectors.
329 Related to the origin of NDIR detector drift in combination with the dual wavelength
330 setup it should be pointed out that changes in the zero concentration measurements can
331 (i) occur erratically especially after transportation of storage, (ii) are not necessarily linear
332 in time with (iii) the slope commonly decreasing over running time or (iv) even changing
333 its sign.

334 The zero correction of a two-beam sensor signal does not cover concentration
335 dependent effects that equate to changes in the characteristics of the NDIR sensor's
336 calibration polynomial. Hence for achieving best accuracies particularly with two-beam
337 NDIR sensors, the sensor in addition to regular zeroings needs to be re-calibrated after
338 deployment at different concentrations.

339 *d. Membrane equilibration*

340 The solution-diffusion model can be used to describe gas transport through a dense, semi-
341 permeable membrane. Assuming a partial pressure gradient between the water phase and
342 the internal gas stream, the first step within the transport process is adsorption of the
343 molecule at the membrane surface. In the case of a sufficiently small gas concentration
344 the dissolution process into the membrane can be explained by the Henry-Dalton Law,
345 which states the linearity between the partial pressure of a gas and the concentration of
346 that gas in solution connected by a temperature, pressure and, in the case of sea water,
347 salinity dependent constant. The dissolution process is followed by diffusion based
348 transport of the molecules within the membrane along the concentration gradient.
349 Outgasing into the headspace again follows the Henry-Dalton Law. This process
350 continues within the membrane of the sensor until partial pressure equilibrium with

respect to every single gas component is achieved. Hence semi-permeable membranes can be used as equilibrators for dissolved gas measurements (McNeil et al. 2006). They enable the application of gas phase based measuring techniques in an aquatic medium. The time limiting and overall response time dominating step within the entire transport process is the diffusion within the membrane material as well as within a boundary layer in front of the membrane. The permeability of a material is a parameter integrating both, the solubility of a gas within the membrane substance as well as its diffusion constant within the membrane according to Fick's Law. Like the solubility and the diffusion coefficient, the permeability is also temperature and pressure dependent as well as concentration independent. The permeabilities of different gases for a given membrane material differ (Robb 1968; Merkel et al. 2000) and hence determine the time constant for the corresponding partial pressure equilibration. The direction of the transport process is defined by the orientation of the individual partial pressure gradient. Silicone, polydimethylsiloxane (PDMS), was chosen as the membrane material due to its high permeability for CO_2 (Merkel et al. 2000).

In addition to all the dissolved gases, water vapor also permeates through the membrane. Its amount within the gas stream is related to the temperature and salinity driven water vapor pressure. The risk of condensation within the headspace and especially within the NDIR absorption path induced by steep gradients of warm to cold water is minimized by the heating of the gas on its way to the NDIR detector. Furthermore the permeability of water vapor is more than a magnitude higher than for CO_2 (Robb 1968), leading to time constants for water vapor equilibration of about 10 s at the given CO_2 response time of about 70 s for this sensor.

Typically silicone layer thicknesses of around 10 µm are used. The thickness is determined during membrane production by permeability measurements. Pure silicone monolayer membranes of this thickness could not be easily handled. Therefore we use thin film composite membranes consisting of the dense silicone layer on top of supporting substructures. In the case of no or minor fouling the membranes can be deployed for several months to years. Cleaning of the membranes with e.g. diluted sulfuric or oxalic acid at pH 2 has successfully been tested. To avoid physical damage of the thin silicone layer mechanical cleaning of the membrane surface should be avoided. Instead the membrane should and can be changed even in the field. The response time of the sensor determined from the flush interval data can also be used to identify organic ongrowth, since heavy fouling slows down the membrane permeation process or the volume rate of pumped water, which both leads to a reduced response time of the sensor.

3. In-water calibration setup

Along with the sensor development we established a laboratory calibration setup for direct underwater pCO_2 calibration (Fig. 3) that can hold up to three sensors simultaneously. An early version of the setup was successfully used in Friedrichs et al. (2010). The setup includes a 120 L insulated and temperature stabilized water tank. The water temperature can be controlled over the temperature range of 0°C to 30°C to within ±0.02 °C. It is filled with de-ionized water. Sodium carbonate and bicarbonate are added in the required quantities in order to mimic the CO_2 buffer system of seawater (DIC:TA ratio) and thereby allow for a better pCO_2 level control. Silver nitrate is added as an anti-foulant. Water is continuously pumped through a reference flow-through pCO_2 system (Körtzinger et al. 1996), which was slightly modified to suit the laboratory conditions.

Additionally it was equipped with drying components to facilitate continuous reference measurements in dry gas. Special care was taken that the return flow of the water from the combined bubble-type/laminar-flow equilibrator into the main tank occurs without flow restrictions and thus without altering the pressure conditions within the equilibrator. Temperature probes within the equilibrator and the main tank are regularly calibrated against a reference probe with an accuracy of ±0.02 °C. The flow-through system is equipped with a bench top IR analyzer (LI-6262 or LI-7000, LI-COR Inc, Lincoln, Nebraska, USA), which is calibrated against 3 primary (certified National Oceanic and Atmospheric Administration (NOAA) standards) or secondary (referenced to NOAA standards) CO_2-in-natural-air standards in the beginning and in the end of each calibration run. Processing of the flow-through system data is carried out according to the procedures described in Dickson et al. (2007) and Pierrot et al. (2009), leading to pCO_2 reference values referred to the water temperature in the tank with an accuracy of 2-3 µatm. During a full calibration run, the pCO_2 of the tank water is altered by pH variation through injection of NaOH or HCl solutions. A new concentration in the tank water is set and resolved by the reference system with a time constant of approx. 150 s. By application of the pH-varying technique a wide pCO_2-range can be realized and calibration steps can be set as desired. Since the overall setup cannot be entirely encapsulated from the surrounding air a small drift of the partial pressures in the tank of typically around 3 µatm hr^{-1} can be observed. Magnitude and timescale of this drift as well as the fact that both, the flow-through system and the underwater sensor, detect this pCO_2 change make this effect negligible with respect to the assumed accuracy of the calibration process. The adjustable range is limited by the measurement range of the IR-

420 analyzer of the flow-through system, which is 3000 µmol mol^{-1} for the dry CO_2 mole
421 fraction in the equilibrated gas stream (xCO_2). It was found that four calibration steps are
422 sufficient for a sensor calibration in the range of 200 to 1000 µatm. The course of a
423 calibration is depicted in Fig. 2.

424 There are several reasons to calibrate the sensor in water against a proven
425 underway system as opposed to a mere dry gas calibration of the IR detector. The fact
426 that some of the following influences are already considered in data processing
427 corrections or their minimization was addressed in sensor design, does not debilitate the
428 following compensatory advantages of an in-water calibration. Firstly, the temperature
429 stabilization including the gas heater used in the sensor does not completely avert the
430 presence of temperature gradients within the instrument's housing, components and gas
431 stream. Hence the temperature stabilization can only minimize the above mentioned
432 possible temperature effects on NDIR sensors. An in-water calibration at a temperature as
433 close as possible to the expected temperature in the field helps to further reduce these
434 signal influences. Secondly, an in-water calibration as described compensates for all
435 effects related to the large absolute humidity present in the sensor's gas stream. These
436 effects are gas-gas-interactions causing band broadening, potential cross sensitivities of
437 the NDIR signal against H_2O due to minor H_2O absorption at the transmitted
438 wavelengths, or H_2O molecule interaction with the cuvette's surface. For a sensor
439 calibration at only one temperature it is deliberately accepted that the humidity related
440 compensations are only entirely compensated for a deployment at a water temperature
441 equal to the calibration temperature. Thirdly, an in-water calibration compares the fully
442 processed signal of the instrument with a reference value. Hence it characterizes the

443 overall instrument including the entire membrane equilibration process of the headspace
444 as identified to be important by Byrne et al. (2010). Any not otherwise considered effects
445 occurring in the sensor's gas stream and behind the membrane are taken care of by an in-
446 water calibration.

447 4. Data processing

448 The dual-beam NDIR detector provides two signals. The raw signal, S_{raw}, corresponds to
449 the transmitted light intensity around the wavelength at which CO_2 efficiently absorbs
450 (4.26 µm) and the reference signal, S_{ref}, expresses the intensity at around 4 µm where
451 practically no relevant absorption occurs. Water vapor is weak absorber at both
452 wavelengths. A continuously referenced sensor signal, the "two-beam signal", is:

$$S_{2beam} = \frac{S_{raw}}{S_{ref}}. \quad (3)$$

453 As a result of the regular zeroing (Z), we obtain "two-beam zero signals" at
454 discrete points in time:

$$S_{2beam,Z} = \frac{S_{raw,Z}}{S_{ref,Z}}. \quad (4)$$

455 Linear interpolation in time between two adjacent $S_{2beam,Z}$ provides zero reference
456 signals for every point in time: $S_{2beam,Z}(t)$.

457 An NDIR signal that is improved by both drift correction (DC) means, dual beam
458 and zeroing, is derived as follows:

$$S_{DC}(t) = \frac{S_{2beam}(t)}{S_{2beam,Z}(t)} \quad (5)$$

459 The final, drift corrected NDIR signal, which is assumed to be directly
460 proportional to the amount of target molecules in the beam path is related to $S_{DC}(t)$.

461 During calibration the flow-through system provides a reference pCO_2 for every
462 calibration step. The pCO_2 equilibrium is assumed to be established in the membrane
463 equilibrator of the sensor at that time. Using data of the peripheral sensors in the gas
464 stream, the xCO_2 in moist air present at the NDIR detector is derived. As the NDIR signal
465 is proportional to the number of molecules in the beam path and not to xCO_2, the
466 reference xCO_2 needs to be density corrected by using data of the additional temperature
467 and pressure sensors built into the gas stream of the pCO_2 sensor. A polynomial of rank 3
468 with a forced zero crossing is then used to calibrate the individual sensor characteristics.
469 It correlates the absorbance signal of the NDIR detector with the corresponding and
470 density corrected xCO_2 in the gas stream (c.f. Fig. 4). Now, all required dependencies are
471 known and the sensor provides the pCO_2 based on the absorbance signal of its NDIR
472 detector in combination with the data of the peripheral sensors in its gas stream. Beside
473 the density correction no other NDIR signal correction addressing a band broadening
474 effect as a consequence of CO_2-H_2O molecule interactions or any other H_2O cross
475 sensitivity is explicitly included in the sensor sided data processing at this point. These
476 aspects are considered through the in-water calibration as mentioned in section 3.
477 Since the consideration of the zeroings requires an interpolation in time, this
478 calculation step is best applied during post processing of field data to obtain a smooth
479 behavior. In order to achieve the best measurement accuracy, changes in the sensor
480 characteristics should also be included into the processing. Therefore an interpolation
481 between the polynomial of a pre-deployment calibration and the polynomial of a post-
482 deployment calibration over the course of the deployment is conducted. We apply an
483 interpolation that is not linear with time, but instead linear with the actual value of the

484 zero signal throughout a deployment, $S_{2beam,Z}(t)$. The pre-deployment polynomial is
485 transformed to the post-deployment polynomial by proportionately using the coefficients
486 of the two polynomials according to the actual zero signal. This approach assumes a
487 causal relationship between the temporally often non-linear change in the zero signal and
488 the change in concentration dependent sensor response.

489 The entire calibration calculations as well as the post processing are accomplished
490 with custom-designed LabVIEW routines (National Instruments, Austin, Texas).

491 5. Field evaluation

492 Field evaluations of the new pCO_2 sensor were carried out in April/May 2010 during a 6-
493 week cruise in the North and South Atlantic (R/V *Polarstern*, ANT-XXVI/4) and in
494 June/July 2011 during a 4-week cruise in the eastern tropical Atlantic (R/V *Maria S.*
495 *Merian*, MSM-18/3; Fig. 5). During these cruises, oligotrophic (i.e., subtropical gyres) as
496 well as mesotrophic regions (e.g., continental shelfs, equatorial upwelling) provided a
497 reasonably wide range in pCO_2 (295 to 430 µatm; c.f. Fig 6. and Fig 7. top panel) and
498 temperature (7.4 to 30.3°C, Fig. 5). Furthermore, strong pCO_2 and temperature gradients
499 were found near hydrographic fronts. Thus, the conditions were ideal for a thorough
500 evaluation of the sensor, which was tested during both cruises in nearly identical
501 underway setups: Seawater, either supplied by the ship's clean seawater supply systems
502 (ANT-XXVI/4) or by a submersible pump installed in the moon pool near the ship's keel
503 (MSM-18/3), was pumped to the laboratory into a thermally insulated flow-through box
504 (80 L volume) at a flow rate of approx. 12 L min^{-1}. Sea surface temperature (SST) and
505 sea surface salinity (SSS) were determined for both cruises at the seawater intake. A
506 sensor package containing the pCO_2 sensor (two units during ANT-XXVI/4, HC1 and

HC2; one unit on MSM-18/3, HC3) and an oxygen optode (Model 3830 or 4330, Aanderaa Data Instruments AS, Bergen, Norway), which also provided the water temperature in the flow-through box with an accuracy of ±0.05°C, were placed in the underway box. Data were binned into 1-min intervals. Since the pCO_2 sensor data were initially stored at 5-s intervals the transformation to the 1-min intervals represents an averaging of typically 12 spot values. Zeroings were carried out every 12 hours. The membrane interface of the pCO_2 sensor was supplied with a constant seawater flow by a SBE 5T pump (Sea-Bird Electronics Inc., Bellevue, Washington). A fully automated pCO_2 underway instrument (GO, General Oceanics, Miami, USA; Pierrot et al. 2009) based on a spray head equilibrator and a LI-7000 CO_2 analyzer was operated in parallel. Throughout the expeditions and beside the deployment in the flow-through box the sensors were additionally used for measurements on a CTD rosette system (HC1 and HC3; part of the data shown in Fiedler et al. 2013) as well as on a surface drifter (HC3; unpublished data).

The two sensors HC1 and HC2 were calibrated at 19.67°C before and after the deployment. HC3 was pre- and post-calibrated at 27.00°C and 26.00°C, respectively.

The averaged sensor data were prepared for processing by filtering for obvious outlier zero values as, for example, caused by improper sensor warm-ups, as well other outliers and data biased through insufficient water supply to the flow-through box. All pCO_2 sensor data recorded during flush and zero intervals were excluded from the comparison with the reference. The data of HC2 obtained between 28th of April and 4th of May were excluded from the comparison as well, as the excessively high water temperature did not allow for temperature stabilization at the calibration control

530 temperature anymore. Although the control temperature within HC1 also temporarily
531 exceeded the set point, no data were removed here, as the unit seemed to be more robust
532 in this respect as compared to HC2.

533 Figures 6 and 7 show the pCO_2 measured by the flow-through reference system as
534 well as the pCO_2 data of the HC1-3 sensors with all datasets corrected to SST for direct
535 comparison (Takahashi et al. 1993). In addition, the pCO_2 differences (ΔpCO_2) between
536 the sensor and the reference ($pCO_{2,GO}$) are plotted vs. time. The three ΔpCO_2 curves for
537 every sensor are related to different drift compensation mechanisms:

538 (i) pre-calibration, no zeroings

539 (ii) pre-calibration + zeroings

540 (iii) pre-calibration + zeroings + post-calibration

541 In the case of (i) only the dual-beam correction is applied and the polynomial of
542 the pre-deployment calibration is used for the entire data set. Since in this case data are
543 processed by referencing all signals to the zeroing carried out during shore-based
544 calibration, large offsets can already occur at the beginning of a deployment due to a
545 sensor drift that occurred during storage and transport or due to measurement conditions
546 that strongly deviate from calibration conditions. Also more or less strong drift behavior
547 is observed over time. When the regular zero correction is carried out as described above
548 (section 4), both initial offsets and drift over the course of the deployment are strongly
549 reduced demonstrating the effectiveness of this first correction. However, even smaller
550 residuals were obtained when both zeroings as well as pre- and the post-deployment
551 calibration polynomials are considered in the post-processing (section 4). Table 2 shows
552 the statistics of the pCO_2 residuals as obtained by this optimized processing routine. In all

three sensor deployments the mean pCO_2 offset to the reference system is within ±3 µatm. With an average pCO_2 residual over all three sensors of -0.6 ± 3.0 µatm (RMSE=3.7 µatm) no systematic offset between pCO_2 sensor and reference system could be found. This indicates that the agreement between sensor and flow-through system pCO_2 is of similar magnitude as the accuracy of the flow-through system which was estimated at 2 µatm (Pierrot et al. 2009). We use the mean RMSE from all three deployments of 3.7 µatm as a conservative estimate of the sensor accuracy. This result is very promising as the sensors were only calibrated at a single water temperature and experienced a large temperature range during deployment (>20°C). We note that during these field tests the sensors ran autonomously and without maintenance but were also used in other tests (e.g., deployments of CTD rosette casts; part of the data shown in Fiedler et al., 2013). For this purpose the instruments had to be restarted several times. This appears to not have affected sensor performance negatively, since sensor HC3 was restarted most frequently but shows the smallest overall offset.

The compensation routines applied, which exclusively rely on data measured by the sensors themselves and the information obtained from calibrations, account well for the signal drift for all 3 sensors. After processing the data do not exhibit significant unaccounted drift behavior. This is even the case for the most strongly drifting sensor HC1, whose signal change over time is also reflected by the change in its calibration polynomials (Fig. 4). Although an NDIR detector drifting as strongly as in the case of HC1 would not pass current quality controls within the manufacturer's production, it is still a good example to demonstrate the effectiveness of the described processing algorithms. We would like to note that sensor HC1 also participated in a different sensor

576 evaluation project (Tamburri et al. 2011). At that time, the sensor also showed a strong
577 drift that could not be adequately compensated for due to lack of the full understanding of
578 the required post-processing steps that is presented here. Although the drift of HC1 could
579 be well corrected for, in the end it still shows a slightly larger mean value and RMSE
580 compared to HC2 and HC3. NDIR detectors that show a smaller zero drift, typically
581 show a smaller concentration dependent signal change over time as well. This conclusion
582 is further corroborated by the observation that a transformation of the pre-deployment
583 into the post-deployment calibration polynomial based on the course of the zero values
584 finally provides a better correction as opposed to a transformation assumed to occur
585 linear in time (data not shown here).

586 In order to identify any remaining issues in the drift corrected pCO_2 sensor data,
587 the ΔpCO_2 residuals were plotted against $pCO_{2,GO}$, SST and pH_2O (Fig. 8). All sensors
588 show a weak correlation with all three parameters ($0.0<R^2<0.6$), which is most clear for
589 sensor HC2 ($0.5<R^2<0.6$). Since $pCO_{2,GO}$, SST and pH_2O are strongly correlated in the
590 field data, the cause of these remaining residual correlations cannot be clearly discerned.
591 Nevertheless, there is indication for a weak NDIR signal dependency on pH_2O. In fact,
592 CO_2-NDIR detectors over-estimate in the presence of water vapor due to pressure
593 broadening effects (McDermitt et al. 1993). Furthermore, the magnitude of this effect
594 increases with pCO_2 and pH_2O. Since the sensor calibrations were only conducted at one
595 temperature and band broadening effects due to varying water vapor concentrations are
596 not considered within the sensor's data processing, this might explain at least part of the
597 dependencies. The fact that HC2 and HC3 show the smallest ΔpCO_2 around the water
598 temperature at which they were calibrated, support this observation. The limitations of

599 the present data set do not allow to further investigate this issue and additional tests have
600 to be carried out to assess the potential for further improvement, e.g., by performing
601 laboratory tests with and calibrations of the pCO_2 sensor at more than one temperature.

602 6. Summary and outlook

603 The development of a new underwater pCO_2 sensor based on membrane equilibration and
604 NDIR spectrometry was described. Special emphasis was put on compensation measures
605 for NDIR sensor drift as well as on the in-water calibration of the sensor. The
606 performance of the pCO_2 sensor was assessed based on surface water field data obtained
607 during two cruises both lasting at least one month and covering a wide range in pCO_2
608 (289 to 445 µatm) and temperature (7.4 to 30.1°C). A wet gas stream within a small
609 underwater sensor represents a demanding environment for NDIR detectors. Against this
610 background the observed mean offset of -0.6 ±3.0 µatm with a RMSE of 3.7 µatm to the
611 pCO_2 reference instrument as obtained through application of a pre- and post-deployment
612 calibration in combination with regular zeroings is a very promising result, especially
613 since the sensors were also used for various other measurements including profiling
614 applications in the water column during the deployments (data not part of this
615 assessment). At a pCO_2 of 400 µatm the observed mean pCO_2 difference corresponds to
616 about 0.2 % and the RMSE to less than 1 %. This favorable result underlines the
617 efficiency of the applied processing algorithms. The acquisition of high-quality field data
618 by the new pCO_2 sensor calls for regular checks of the sensor parameters gas
619 temperature, pressure, RH and control temperature to guarantee optimal functioning of
620 the sensor. In addition, regular zero gas measurements need to be carried out at least
621 every 12 h under deployment conditions as a drift correction means beside the inherent

single-beam dual wavelength setup of the sensor. To properly apply the zero information during post processing measurement data should always be flanked by zeroings. Thirdly, in order to also account for the concentration dependant effects on zero and dual beam corrected signals, the sensor needs to be re-calibrated at different pCO_2 levels on a time scale of several months to a year to achieve the highest accuracies through data post processing. A water calibration as presented in this paper at a temperature close to the expected water temperatures in the field is beneficial. Nevertheless, the RMSE found within this work is based on field data obtained under conditions where water temperatures deviated by ±10°C from the calibration temperature.

The assessment given here represents an important milestone for the development of the sensor. The procedures discussed are planned to be further automated and implemented into data processing routines. The next development steps include investigation of potential improvements with respect to NDIR data processing and the laboratory calibration routines to identify and compensate for minor signal dependencies on water vapor and on changes in gas matrix composition as caused by e.g. strongly varying oxygen concentrations. Moreover the long-term stability during deployments on moorings and profiling buoys in the water column will be investigated as well as the sensor performance on different moving platforms analyzed. Especially the latter has been simplified by a recently released smaller and faster version of the HydroC.

Acknowledgments.

The authors would like to thank all members of the "(C)O_2" working group at the GEOMAR as well as Gernot Friedrichs from the CAU for fruitful discussions and helpful advice. Furthermore, we thank the CONTROS team for their support in this development project. We explicitly acknowledge Christian Rettich for his assistance especially during the construction of the first prototypes as well as Claus Hinz and Matthias Lunge for valuable help with laboratory experiments. Janna Bohlen and Christoph Kirbach are thanked for commenting on the manuscript. We would also like to thank captains and crews of R/V *Polarstern* and of *Maria S. Merian* for assistance. This work was partly funded by the SAW project OCEANET of the Leibniz Association (2008-2010) and by the SOPRAN project of the German Federal Ministry of Education and Research (grants 03F0462A and 03F0611A).

References

Byrne, R. H., and W. Yao, 2008: Procedures for measurement of carbonate ion concentrations in seawater by direct spectrophotometric observations of Pb(II) complexation. *Mar. Chem.*, **112**, 128–135, doi:10.1016/j.marchem.2008.07.009.

Byrne, R. H., X. Liu, and E. A. Kaltenbacher, 2002: Spectrophotometric measurement of total inorganic carbon in aqueous solutions using a liquid core waveguide. *Anal. Chim. Acta*, **451**, 221–229, doi:10.1016/S0003-2670(01)01423-4.

Byrne, R. H. and Coauthors, 2010: Sensors and Systems for in situ Observations of Marine Carbon Dioxide System Variables. *Proceedings of OceanObs'09: Sustained Ocean Observations and Information for Society*, J. Hall, D.E. Harrison, and D. Stammer, Eds., Venice, Italy, ESA Publication WPP-306.

DeGrandpre, M. D., T. R. Hammar, S. P. Smith, and F. L. Sayles, 1995: In-Situ Measurements of Seawater pCO_2. *Limnol. Oceanogr.*, **40**, 969–975.

Dickson, A. G., C. L. Sabine, and J. R. Christian, eds., 2007: *Guide to best practices for ocean CO_2 measurements*. PICES Special Publication 3.

Doney, S. C., V. J. Fabry, R. A. Feely, and J. A. Kleypas, 2009: Ocean Acidification: The Other CO_2 Problem. *Ann. Rev. Mar. Sci.*, **1**, 169–192, doi:10.1146/annurev.marine.010908.163834.

Fiedler, B., P. Fietzek, N. Vieira, P. Silva, H. C. Bittig, and A. Körtzinger, 2013: In situ CO_2 and O_2 measurements on a profiling float. *J. Atmos. Oceanic Technol.*, **30**, 112–126.

Fietzek, P., S. Kramer, and D. Esser, 2011: Deployment of the HydroC^{TM} (CO_2/CH_2) on stationary and mobile platforms - Merging the trends in the field of platform and sensor development. *Proceedings of Oceans 11 MTS/IEEE Conference, 19-22 Sept. 2011*, Kona, Hawaii, USA, 1–9.

Friedrichs, G., J. Bock, F. Temps, P. Fietzek, A. Körtzinger, and D. W. R. Wallace, 2010: Toward continuous monitoring of seawater $^{13}CO_2$/ $^{12}CO_2$ isotope ratio and pCO_2: Performance of cavity ringdown spectroscopy and gas matrix effects. *Limnol. Oceanogr.: Methods*, **8**, 539–551, doi:10.4319/lom.2010.8.539.

Gruber, N. and Coauthors, 2010: Toward an Integrated Observing System for Ocean Carbon and Biogeochemistry at a Time of Change. *Proceedings of OceanObs'09: Sustained Ocean Observations and Information for Society*, J. Hall, D.E. Harrison, and D. Stammer, Eds., Venice, Italy, ESA Publication WPP-306.

688 IPCC, 2005: *IPCC special report on carbon dioxide capture and storage*. B. Metz, O.
689 Davidson, H. De Coninck, M. Loos, and L. Meyer, Eds. Cambridge University
690 Press.

691 Johnson, K. S. and Coauthors, 2009: Observing biogeochemical cycles at global scales
692 with profiling floats and gliders: prospects for a global array. *Oceanography*, **22**,
693 216–224.

694 Körtzinger, A., H. Thomas, B. Schneider, N. Gronau, L. Mintrop, and J. C. Duinker,
695 1996: At-sea intercomparison of two newly designed underway pCO_2 systems -
696 encouraging results. *Mar. Chem.*, **52**, 133–145.

697 Körtzinger, A. and Coauthors, 2000: The international at-sea intercomparison of fCO_2
698 systems during the RV Meteor Cruise 36/1 in the North Atlantic Ocean. *Mar.*
699 *Chem.*, **72**, 171–192, doi:10.1016/S0304-4203(00)00080-3.

700 Lefèvre, N., J. P. Ciabrini, G. Michard, B. Brient, M. DuChaffaut, and L. Merlivat, 1993:
701 A new optical sensor for pCO_2 measurements in seawater. *Mar. Chem.*, **42**, 189–
702 198, doi:10.1016/0304-4203(93)90011-C.

703 Martz, T. R., J. G. Connery, and K. S. Johnson, 2010: Testing the Honeywell Durafet for
704 seawater pH applications. *Limnology And Oceanography Methods*, **8**, 172–184,
705 doi:10.4319/lom.2010.8.172.

706 McDermitt, D. K., J. M. Welles, and R. D. Eckles, 1993: Effects of temperature, pressure
707 and water vapor on gas phase infrared absorption by CO_2. *LI-COR, Inc, Lincoln,*
708 *USA.*, 1–5.

709 McNeil, C., E. D'Asaro, B. Johnson, and M. Horn, 2006: A Gas Tension Device with
710 Response Times of Minutes. *J. Atmos. Oceanic Technol.*, **23**, 1539,
711 doi:10.1175/JTECH1974.1.

712 Merkel, T. C., V. I. Bondar, K. Nagai, B. D. Freeman, and I. Pinnau, 2000: Gas sorption,
713 diffusion, and permeation in poly(dimethylsiloxane). *J. Polym. Sci., Part B: Polym.*
714 *Phys.*, **38**, 415–434, doi:10.1002/(SICI)1099-0488(20000201)38:3<415::AID-
715 POLB8>3.0.CO;2-Z.

716 Millero, F. J., 2007: The marine inorganic carbon cycle. *Chem. Rev.*, **107**, 308–341,
717 doi:10.1021/cr0503557.

718 Pfeil, B. and Coauthors, 2013: A uniform, quality controlled Surface Ocean CO_2 Atlas
719 (SOCAT). *Earth Syst. Sci. Data*, 125–143, doi:10.5194/essd-5-125-2013.

720 Pierrot, D. and Coauthors, 2009: Recommendations for autonomous underway pCO_2
721 measuring systems and data-reduction routines. *Deep-Sea Res., Part II*, **56**, 512–
722 522, doi:10.1016/j.dsr2.2008.12.005.

723 Robb, W. L., 1968: Thin silicone membranes - Their permeation properties ans some
724 applications. *Annals New York Academy of Science*, 119–137.

725 Roemmich, D., G. C. Johnson, S. Riser, R. Davis, and J. Gilson, 2009: The Argo
726 Program: observing the global ocean with profiling floats. *Oceanography*, **22**, 34–
727 43.

728 Rogner, H. H., D. Zhou, R. Bradley, P. Crabbé, O. Edenhofer, B. Hare (Australia), L.
729 Kuijpers, and M. Yamaguchi, 2007: *Introduction. In Climate Change 2007:*
730 *Mitigation. Contribution of Working Group III to the Fourth Assessment Report of*
731 *the Intergovernmental Panel on Climate Change*. Cambridge University Press.

732 Sabine, C. L. and Coauthors, 2004: The Oceanic Sink for Anthropogenic CO_2. *Science*,
733 **305**, 367–371.

734 Saderne, V., P. Fietzek, and P. M. J. Herman, 2013: Extreme variations of pCO_2 and pH
735 in a macrophyte meadow of the Baltic Sea in summer: evidence of the effect of
736 photosynthesis and local upwelling. *PLoS ONE*, **8**, e62689,
737 doi:10.1371/journal.pone.0062689.

738 Seidel, M. P., M. D. DeGrandpre, and A. G. Dickson, 2008: A sensor for in situ
739 indicator-based measurements of seawater pH. *Mar. Chem.*, **109**, 18–28,
740 doi:10.1016/j.marchem.2007.11.013.

741 Severinghaus, J. W., and A. F. Bradley, 1958: Electrodes for Blood pO_2 and pCO_2
742 Determination. *J. Appl. Physiol.*, **13**, 515–520.

743 Stow, R. W., R. F. Baer, and B. F. Randall, 1957: Rapid measurement of the tension of
744 carbon dioxide in blood. *Archives of physical medicine and rehabilitation*, **38**, 646–
745 650.

746 Takahashi, T., 1961: Carbon dioxide in the atmosphere and in Atlantic Ocean water. *J.*
747 *Geophys. Res.*, **66**, 477–494.

748 Takahashi, T., J. Olafsson, J. G. Goddard, D. W. Chipman, and S. C. Sutherland, 1993:
749 Seasonal variation of CO_2 and nutrients in the high-latitude surface oceans: A
750 comparative study. *Global Biogeochem. Cycles*, **7**, 843–878.

751 Takahashi, T. and Coauthors, 2009: Climatological mean and decadal change in surface
752 ocean pCO_2, and net sea–air CO_2 flux over the global oceans. *Deep-Sea Res., Part*
753 *II*, **56**, 554–577, doi:10.1016/j.dsr2.2008.12.009.

754 Tamburri, M. N. and Coauthors, 2011: Alliance for Coastal Technologies: Advancing
755 Moored pCO_2 Instruments in Coastal Waters. *Mar. Technol. Soc. J.*, **45**, 43–51,
756 doi:10.4031/MTSJ.45.1.4.

757 Wang, Z. A., X. Liu, R. H. Byrne, R. Wanninkhof, R. E. Bernstein, E. A. Kaltenbacher,
758 and J. Patten, 2007: Simultaneous spectrophotometric flow-through measurements
759 of pH, carbon dioxide fugacity, and total inorganic carbon in seawater. *Anal. Chim.*
760 *Acta*, **596**, 23–36.

761 Watson, A. J. and Coauthors, 2009: Tracking the variable North Atlantic sink for
762 atmospheric CO_2. *Science*, **326**, 1391–1393, doi:10.1126/science.1177394.

763 Weiss, R. F., 1974: Carbon dioxide in water and seawater: the solubility of a non-ideal
764 gas. *Mar. Chem.*, **2**, 203–215.

765 Wiegleb, G. and Coauthors, 2001: *Industrielle Gasssensorik: Messverfahren -*
766 *Signalverarbeitung - Anwendungstechnik - Prüfkriterien*. G. Wiegleb, Ed. expert-
767 Verlag, Renningen.

768

769

List of Figures

TABLE 1. Specifications of the developed pCO_2 sensor as used during the deployments discussed in this paper. The specifications of the currently available sensor model differ from these values with respect to size and power consumption. The power required for the temperature stabilization as well as the warm-up duration depend on the actual water temperature, the chosen control temperature as well as on the thickness of the insulation material. The given warm-up times correspond to 24 V supply voltage in 20°C water and to 12 V supply voltage in 3°C water. Please refer to the text for further details regarding the warm-up and the zeroing interval. The response times refer to the usage of two different pump models at 20°C water temperature. The pump SBE 5T has a flow rate of approx. 105 mL s^{-1}, while the smaller model, SBE 5M, provides a flow rate of approx. 35 mL s^{-1}.

TABLE 2. Statistics of the ΔpCO_2 residuals for all three field deployments of the pCO_2 sensor with mean, standard deviation, σ, and root mean square error, RMSE, for a total of n observations. Also shown is the mean of all three deployments.

FIG. 1. Drawing of the pCO_2 sensor as used in the present study (upper panel). The sensor is equipped with a water pump (SBE 5T) and a flow-head. The lower panel shows a schematic drawing of the sensor. Partial pressure equilibration occurs at the planar, semi-permeable membrane separating the water from the internal head space of approx. 20 mL. A pump continuously circulates the gas between the membrane equilibrator, a heater and the NDIR detector. Valves can be toggled to realize a zero gas measurement by guiding

793 the gas stream through a soda lime cartridge instead of through the membrane
794 equilibrator.
795
796 FIG. 2. Course of a calibration carried out at a constant water temperature within the
797 calibration setup described in the text. The absorbance NDIR signal shown in arbitrary
798 units is dual-beam and zero corrected. Also shown is the CO_2 mole fraction (xCO_2)
799 measured by the reference flow-through system. The numbers 1 – 4 indicate the
800 calibrations steps and "Z", "F" and "M" mark the sensor intervals: zero, flush and
801 measure.
802
803 FIG. 3. In-water pCO_2 sensor calibration setup. One water pump is used to allow for
804 sufficient mixing of the water in the tank, dispersion of the injected acid and base as well
805 as to provide water to the reference flow-through system, which is installed in a bypass
806 and whose NDIR unit is regularly calibrated with reference gases.
807
808 FIG. 4. Calibration polynomials of sensor HC1 before and after the deployment on R/V
809 *Polarstern*. The absorbance NDIR signal is calibrated against the xCO_2 within the
810 sensor's gas stream obtained according to the text. The polynomials match well the
811 sensor's response characteristics (R^2 in both cases >0.999). A concentration dependent
812 change in the sensor characteristics between the different points in time (i.e., before and
813 after deployment) of the calibrations is clearly visible in this example for a strongly
814 drifting NDIR sensor.
815

816 FIG. 5. The cruise track of R/V *Polarstern* cruise ANT-XXVI/4 and of R/V *Maria S.*
817 *Merian* cruise MSM-18/3 (left) as well as the encountered sea surface salinity and
818 temperature (right panel). R/V *Polarstern* sailed from Germany to Chile and R/V *Maria*
819 *S. Merian* from Cape Verde to Gabon.
820
821 FIG. 6. pCO_2 data obtained by the GO-system as well as two HydroC sensors, HC1 and
822 HC2, during ANT-XXVI/4. The top panel shows the absolute values, while the middle
823 and bottom panel show the differences between the HydroC-pCO_2 and the reference
824 (ΔpCO_2) over time for three different processing methods in order to visualize the
825 potential of different drift compensation mechanisms (refer to text). The black curve of
826 HC1 and HC2 represent the final drift corrected and post-processed signal. Refer to text
827 for further details on the different processing methods as well as on the peculiarities of
828 strongly drifting HC1.
829
830 FIG. 7. The pCO_2 trace during MSM-18/3 measured by the GO reference pCO_2 system,
831 and a HydroC sensor, HC3 (top panel). The lower panel shows the pCO_2 residuals
832 between the HydroC and the reference (ΔpCO_2) for three different drift compensation
833 scenarios. The black curve in the lower panel represents the final drift corrected and post-
834 processed signal.
835
836 FIG. 8. In the top row the residuals of HC1 are plotted over the reference pCO_2 (left), the
837 SST (middle) and over the pH_2O as measured within the internal gas stream close to the
838 NDIR detector (right). The middle and the bottom row show the same parameter plots for

839 HC2 and HC3, respectively. Although not statistically significant in all cases, a general
840 positive correlation with all three parameters can be made out and is further discussed in
841 the text.
842

TABLE 1. Specifications of the developed pCO_2 sensor as used during the deployments discussed in this paper. The specifications of the currently available sensor model differ from these values with respect to size and power consumption. The power required for the temperature stabilization as well as the warm-up duration depend on the actual water temperature, the chosen control temperature as well as on the thickness of the insulation material. The given warm-up times correspond to 24 V supply voltage in 20°C water and to 12 V supply voltage in 3°C water. Please refer to the text for further details regarding the warm-up and the zeroing interval. The response times refer to the usage of two different pump models at 20°C water temperature. The pump SBE 5T has a flow rate of approx. 105 mL s^{-1}, while the smaller model, SBE 5M, provides a flow rate of approx. 35 mL s^{-1}.

Measurement principle	IR absorption measurement in a membrane equilibrated headspace
Detector	Single beam dual wavelength NDIR detector; zeroings at desired intervals
Housing, dimensions	Cylindrical titanium housing, 90 x 530 mm (without connector)
Depth capability	2000 m (standard)
Weight	5.5 kg in air, approx. 2.6 kg in water
Operating temperature	3 – 30°C
Supply voltage	11-24 VDC
Power requirements	<3 W for the detector and all the electronics, + <1 W – 3.5 W for temperature stabilization, + <6 W during warm-up for 2 – 30 min,

	+ 4 W during zeroing, + water pump: 7 W or 1.5 W (pump SBE 5T and 5M, respectively)
Sampling rate	≤ 1 Hz
Response time ($t_{63\%}$)	Approx. 70 s or 130 s (pump SBE 5T and 5M, respectively)
Measurement range	200 µatm – 1000 µatm (standard)

854

855 TABLE 2. Statistics of the ΔpCO_2 residuals for all three field deployments of the pCO_2
856 sensor with mean, standard deviation, σ, and root mean square error, RMSE, for a total of
857 n observations. Also shown is the mean of all three deployments.

Sensor	Mean (µatm)	σ (µatm)	RMSE (µatm)	n
HC1	-3.1	2.9	4.2	24791
HC2	1.8	3.4	3.9	24163
HC3	-0.7	2.8	2.8	12770
Overall mean	-0.6	3.0	3.7	

858

859

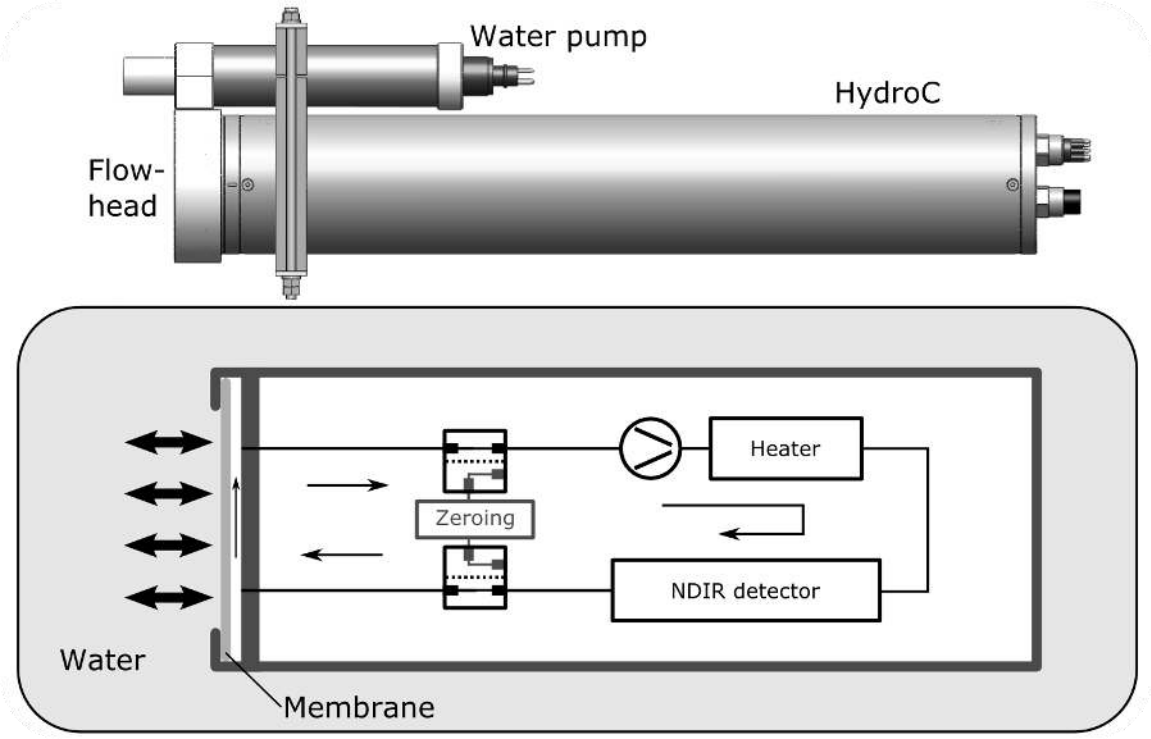

860

861 FIG. 1. Drawing of the pCO_2 sensor as used in the present study (upper panel). The sensor
862 is equipped with a water pump (SBE 5T) and a flow-head. The lower panel shows a
863 schematic drawing of the sensor. Partial pressure equilibration occurs at the planar, semi-
864 permeable membrane separating the water from the internal head space of approx. 20 mL.
865 A pump continuously circulates the gas between the membrane equilibrator, a heater and
866 the NDIR detector. Valves can be toggled to realize a zero gas measurement by guiding
867 the gas stream through a soda lime cartridge instead of through the membrane
868 equilibrator.

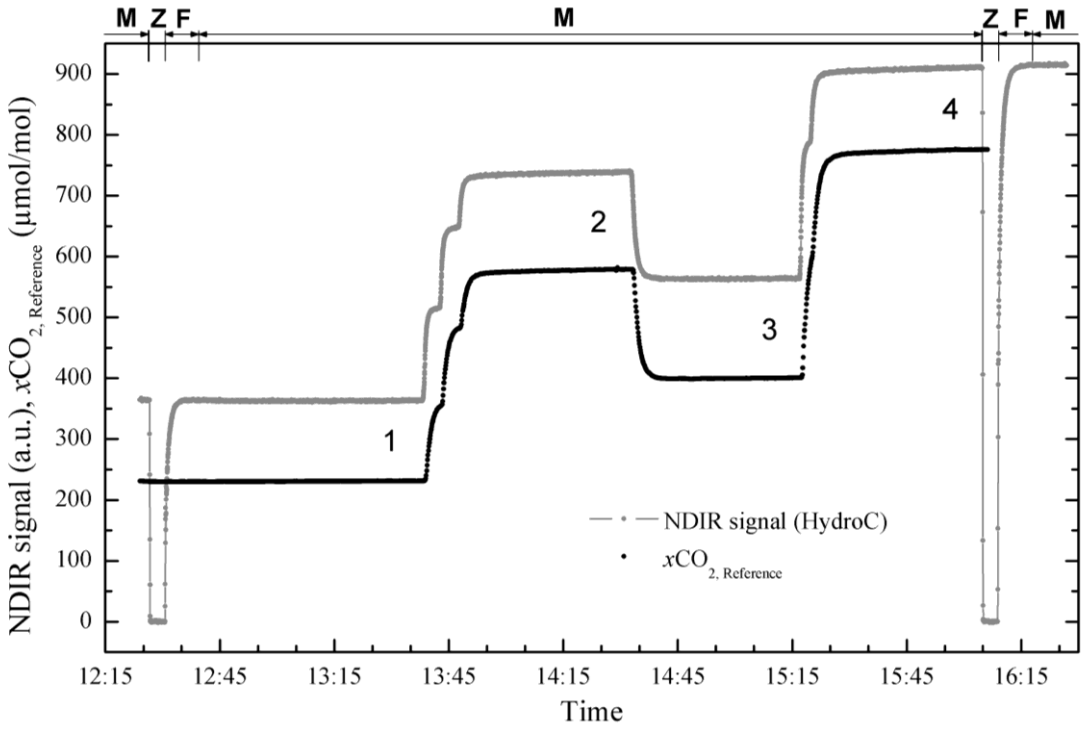

869

870 FIG. 2. Course of a calibration carried out at a constant water temperature within the
871 calibration setup described in the text. The absorbance NDIR signal shown in arbitrary
872 units is dual-beam and zero corrected. Also shown is the CO_2 mole fraction (xCO_2)
873 measured by the reference flow-through system. The numbers 1 – 4 indicate the
874 calibrations steps and "Z", "F" and "M" mark the sensor intervals: zero, flush and
875 measure.

876

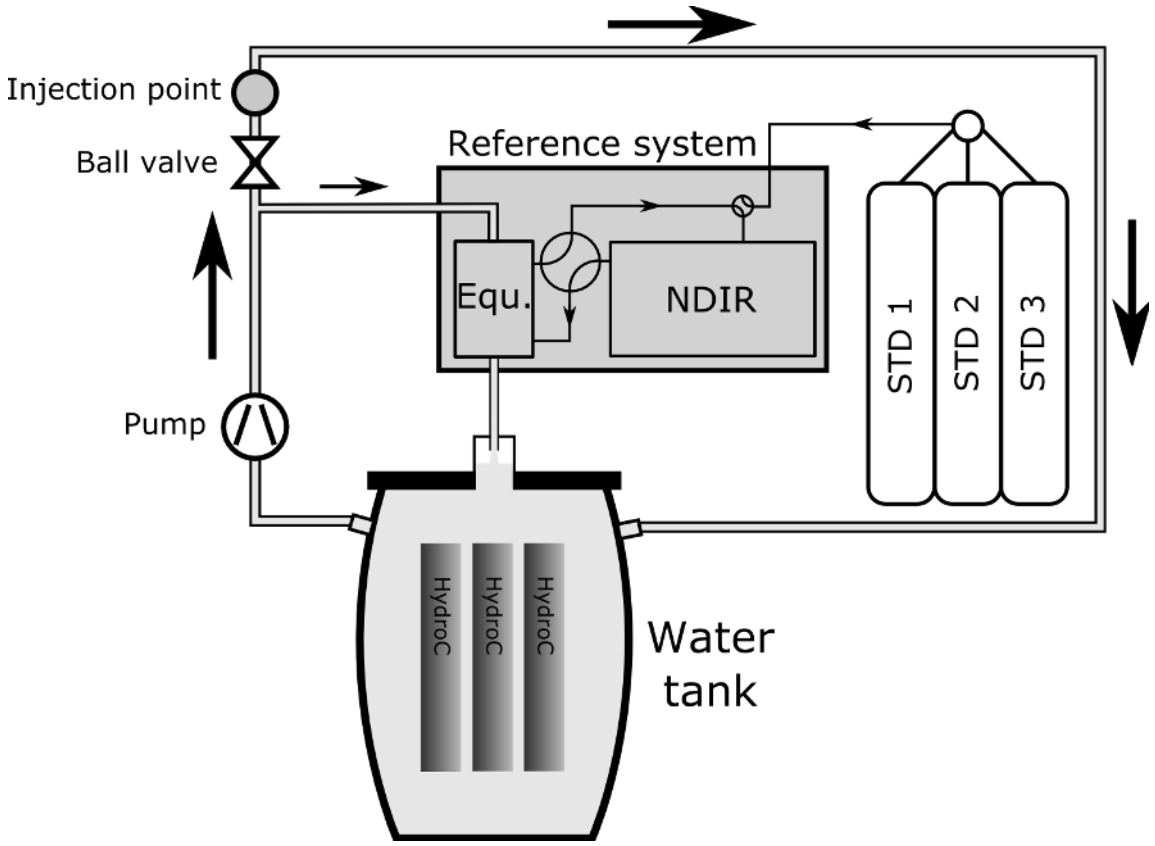

877

878 FIG. 3. In-water pCO_2 sensor calibration setup. One water pump is used to allow for
879 sufficient mixing of the water in the tank, dispersion of the injected acid and base as well
880 as to provide water to the reference flow-through system, which is installed in a bypass
881 and whose NDIR unit is regularly calibrated with reference gases.

882

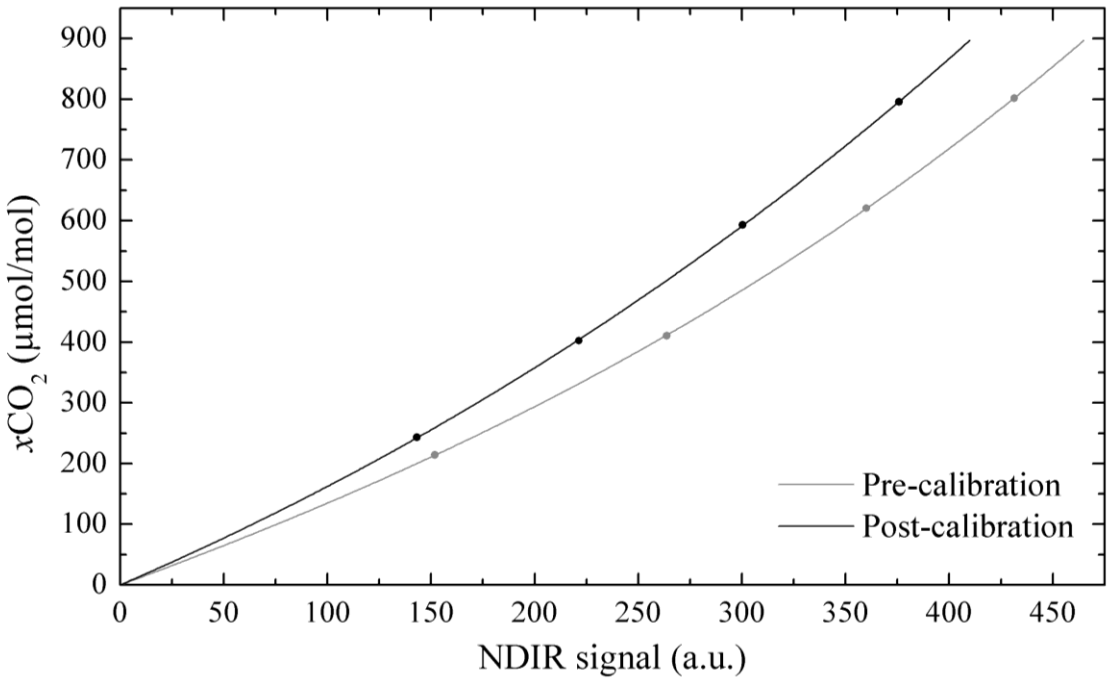

883

884 FIG. 4. Calibration polynomials of sensor HC1 before and after the deployment on R/V
885 *Polarstern*. The absorbance NDIR signal is calibrated against the xCO_2 within the
886 sensor's gas stream obtained according to the text. The polynomials match well the
887 sensor's response characteristics (R^2 in both cases >0.999). A concentration dependent
888 change in the sensor characteristics between the different points in time (i.e., before and
889 after deployment) of the calibrations is clearly visible in this example for a strongly
890 drifting NDIR sensor.

891

892

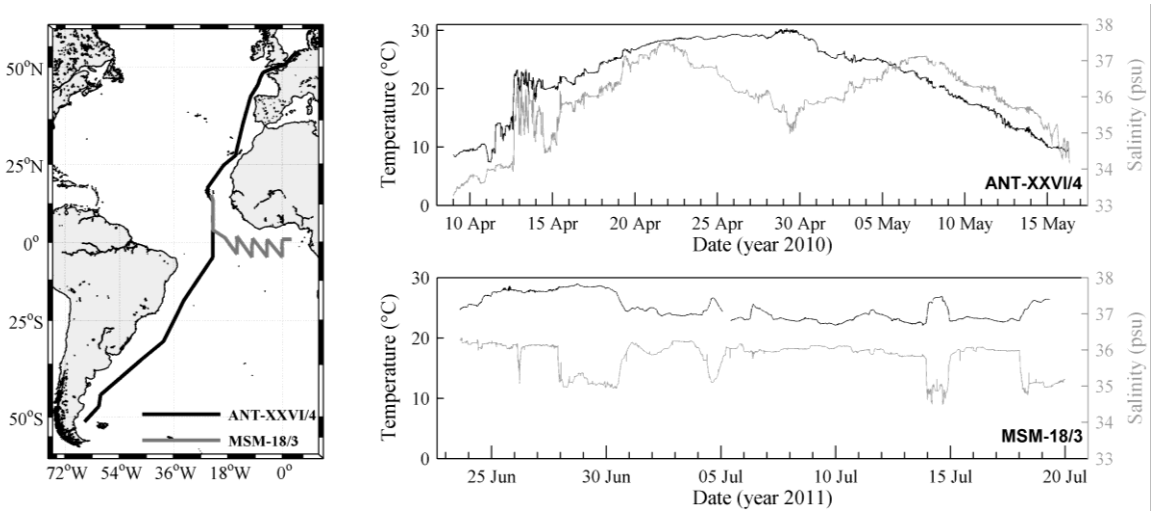

893

894 FIG. 5. The cruise track of R/V *Polarstern* cruise ANT-XXVI/4 and of R/V *Maria S.*

895 *Merian* cruise MSM-18/3 (left) as well as the encountered sea surface salinity and

896 temperature (right panel). R/V *Polarstern* sailed from Germany to Chile and R/V *Maria*

897 *S. Merian* from Cape Verde to Gabon.

898

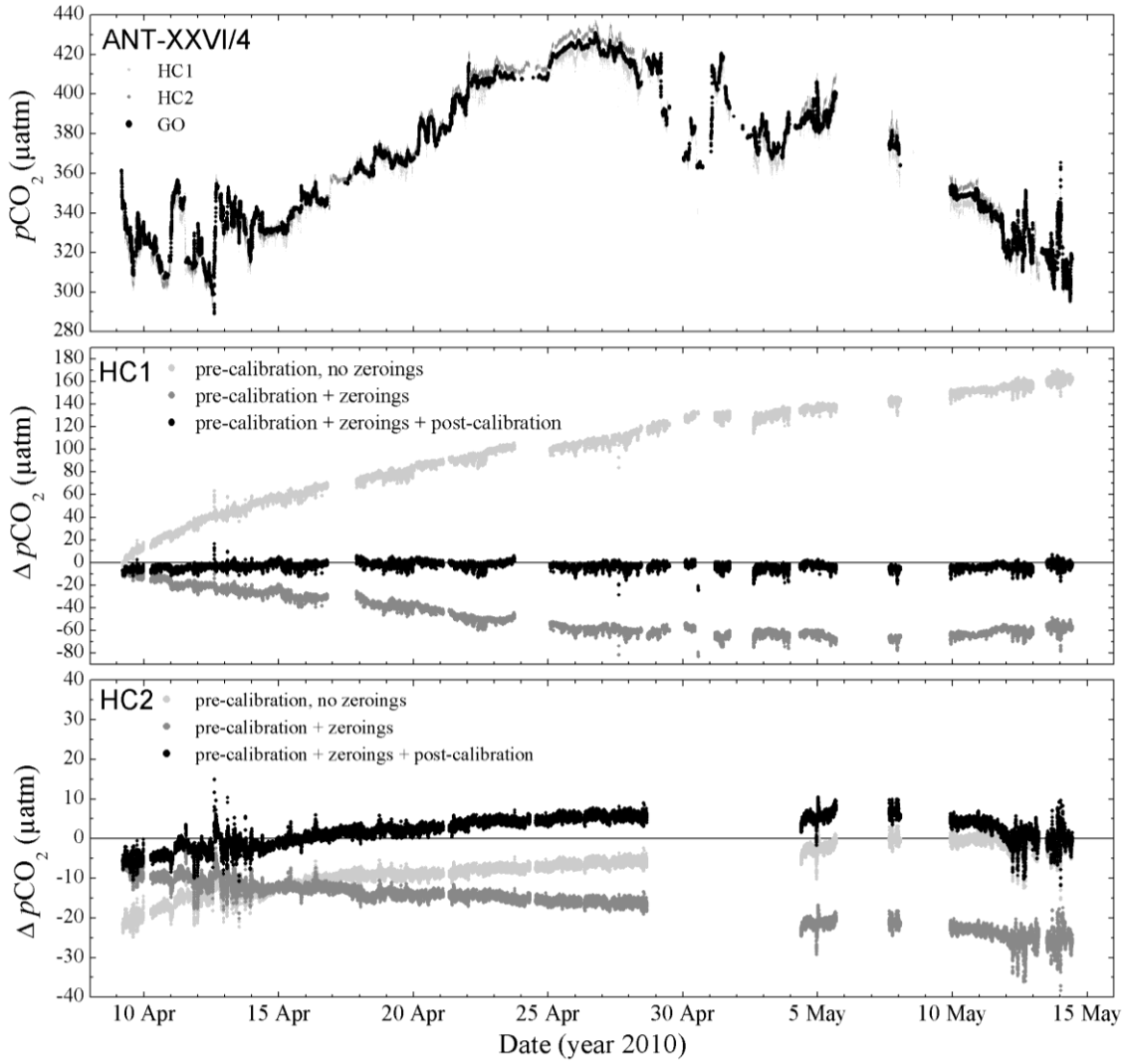

899

900 FIG. 6. pCO_2 data obtained by the GO-system as well as two HydroC sensors, HC1 and
901 HC2, during ANT-XXVI/4. The top panel shows the absolute values, while the middle
902 and bottom panel show the differences between the HydroC-pCO_2 and the reference
903 (ΔpCO_2) over time for three different processing methods in order to visualize the
904 potential of different drift compensation mechanisms. The black curve of HC1 and HC2
905 represent the final drift corrected and post-processed signal. Refer to text for further
906 details on the different processing methods as well as on the peculiarities of strongly
907 drifting HC1.

908

909

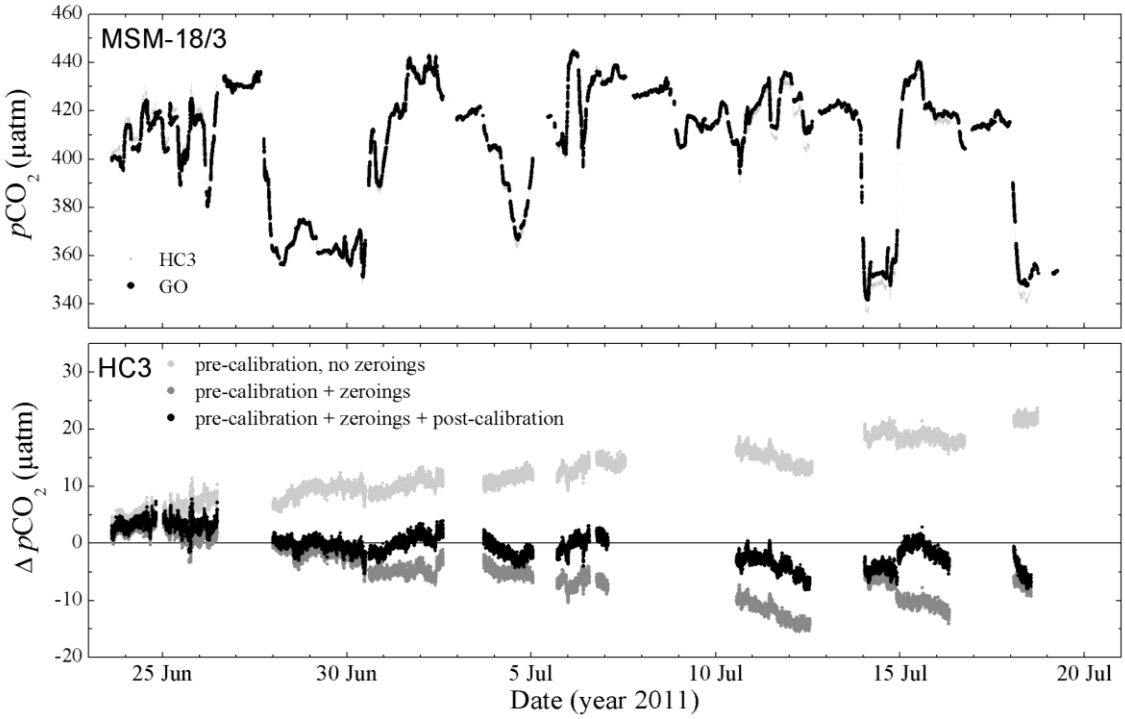

910

911 FIG. 7. The pCO_2 trace during MSM-18/3 measured by the GO reference pCO_2 system,
912 and a HydroC sensor, HC3 (top panel). The lower panel shows the pCO_2 residuals
913 between the HydroC and the reference (ΔpCO_2) for three different drift compensation
914 scenarios. The black curve in the lower panel represents the final drift corrected and post-
915 processed signal.

916

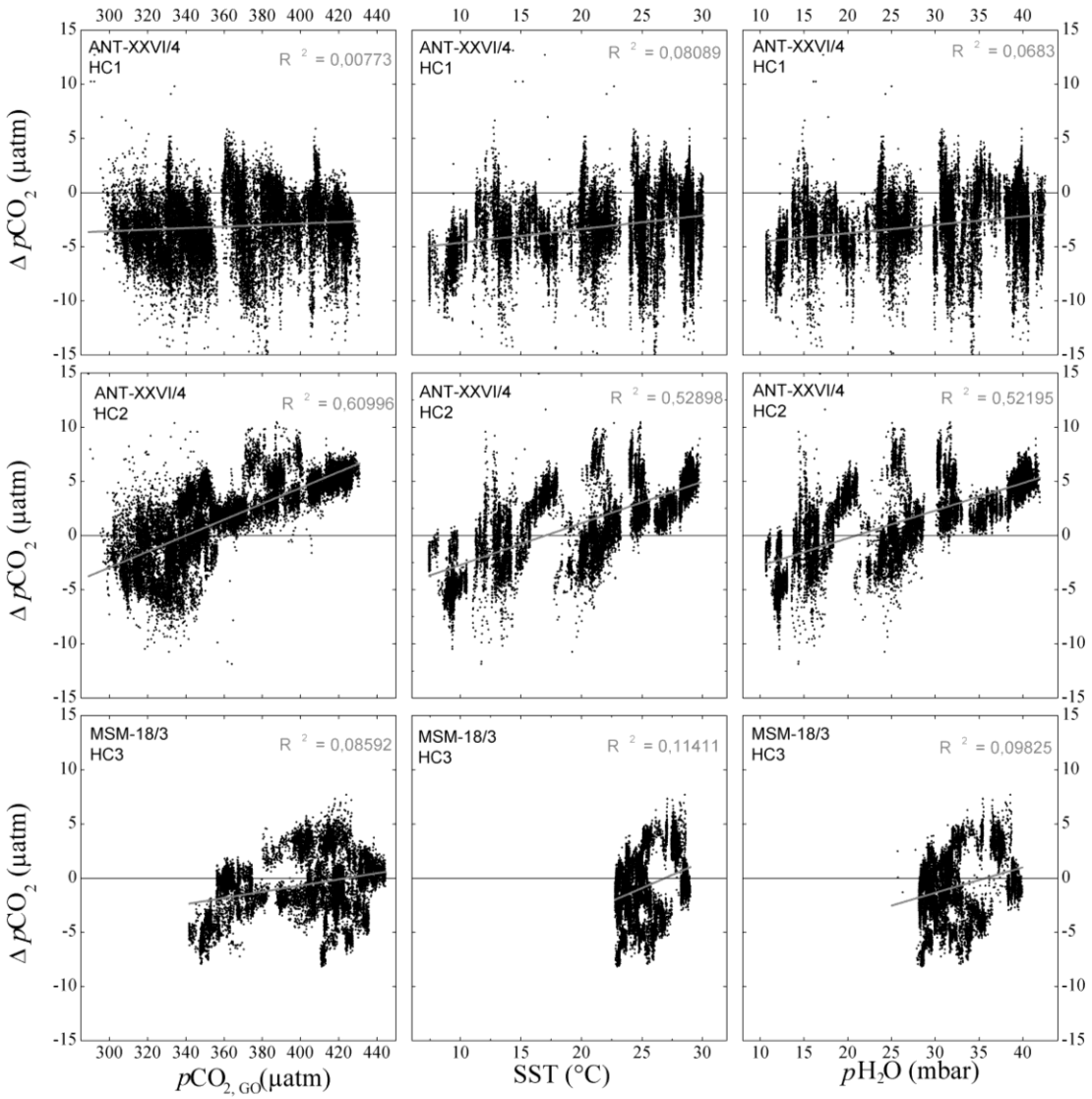

FIG. 8. In the top row the residuals of HC1 are plotted over the reference pCO_2 (left), the SST (middle) and over the pH_2O as measured within the internal gas stream close to the NDIR detector (right). The middle and the bottom row show the same parameter plots for HC2 and HC3, respectively. Although not statistically significant in all cases, a general positive correlation with all three parameters can be made out and is further discussed in the text.